Robust Beamforming and Outage Performance of Uplink Multiuser Satellite-Aerial-Terrestrial Networks With Mixed RF-FSO Channels

Xiaoyu Liu, Chenwei Gu, Kefeng Guo, *Member, IEEE*, Ming Cheng, Min Lin, *Member, IEEE*, and Wei-Ping Zhu, *Senior Member, IEEE*

***Abstract*—In this paper, we investigate the uplink transmission in a satellite-aerial-terrestrial network (SATN), where an aerial platform acts as an amplify-and-forward relay assisting the communication between multiple users and satellite. The users send messages to the aerial relay via radio frequency (RF) links, which are then forwarded to the satellite through a free-space optical (FSO) link. By assuming that the angle-of-arrival based imperfect channel state information of each user is known at the aerial platform, we propose a beamforming scheme to maximize the minimum average signal-to-interference-plus-noise ratio of the users. Due to the mathematical intractability, we design an iterative algorithm to obtain the optimal beamforming vector for the RF link. Furthermore, by considering that the FSO link experiences the Málaga fading with non-zero boresight pointing error and the RF links follow Nakagami-m fading, we derive an analytical expression for the outage probability of the considered SATN. Finally, computer simulation is conducted to validate our theoretical analysis. It is shown that the proposed algorithm can improve the system performance and robustness compared to existing works.**

***Index Terms*—Mixed RF-FSO channels, uplink transmission, outage probability, robust beamforming, satellite-aerial-terrestrial network.**

I. Introduction

Due to the rapid development of smart mobile devices, the current terrestrial communication system is facing many challenges, such as higher data rates, better quality of service, and wider network coverage [1]. To meet those challenges in terrestrial networks, aerial communication is proposed as a promising solution for its easy deployment, high flexibility, and large coverage [2]. Unmanned aerial vehicles can be used as aerial relays to expand the radio coverage for the terrestrial users [3], and collect data for the internet-of-things (IoTs) [4]. Despite the promising benefits brought by aerial platforms, the explosive growth of IoT devices makes the aerial platform connection using backhaul/fronthaul a challenging issue [5]. Because of its inherent large footprint, satellite provides the possibility of connecting the aerial communication for long distance, and furthermore acts as backhaul to the core network [6]–[9]. Thus, the satellite-aerial-terrestrial network (SATN) has attracted increasing attention [10]–[12]. In industry, the ABSOLUTE Project completed the proof of SATN architecture implementations and realistic demonstration [11]. Moreover, the system performance of SATN can be greatly enhanced by employing beamforming (BF) technology to achieve optimum receive and transmit BF vectors at the aerial platform [12]. However, since the radio frequency (RF) spectrum is overcrowded, the conventional RF link between the aerial platform and satellite will be unable to meet the high data rate requirement in the future.

Due to its high bandwidth, free spectrum allocation, and high security, free-space optical (FSO) communication is considered as a potential solution to the spectrum scarcity problem [13]. Note that FSO link is not suitable for the aerial-terrestrial communication because the line-of-sight (LoS) link between the aerial and the moving user could easily be blocked by obstacles, such as buildings and trees, etc. Unlike the aerial-terrestrial link, the LoS path always exists in satellite-aerial link, which is suitable for and in favor of the FSO transmission [14]. Meanwhile, the FSO can meet the high-capacity requirement of the satellite-aerial link to forward a high volume of data by the aerial platform to the satellite [15]. Therefore, a mixed RF-FSO architecture has emerged as a viable solution for SATN.

A mixed RF-FSO network consists of RF and FSO links and normally employs cooperative relay protocol to extend the coverage area and enhance the reliability. In [16], an asymmetric dual-hop relay system was studied for the first time. By considering the pointing errors in the FSO link, the authors in [17] then studied a fixed-gain amplify-and-forward (AF)-based dual-hop RF-FSO network and analyzed the system

Manuscript received May 4, 2021; revised July 7, 2021; accepted July 14, 2021. Date of publication July 21, 2021; date of current version August 10, 2021. This work was supported in part by the Key International Cooperation Research Project under Grant 61720106003, in part by the National Natural Science Foundation of China under Grant 62001517, in part by the Shanghai Aerospace Science and Technology Innovation Foundation under Grant SAST2019-095, in part by NUPTSF under Grant NY220111, in part by the Research Project of Science and Technology on Complex Electronic System Simulation Laboratory under Grants DXZT-JC-ZZ-2019-005 and DXZT-JC-ZZ-2019-009, and in part by Postgraduate Research & Practice Innovation Program of Jiangsu Province under Grant KYCX20_0724. *(Corresponding author: Min Lin.)*

Xiaoyu Liu, Chenwei Gu, Ming Cheng, and Min Lin are with the College of Telecommunications and Information Engineering, Nanjing University of Posts and Telecommunications, Nanjing 210003, China (e-mail: 2019010102@njupt.edu.cn; 15706290291@139.com; mingcheng@njupt.edu.cn; linmin@njupt.edu.cn).

Kefeng Guo is with the School of Space Information, Space Engineering University, Beijing 101416, China (e-mail: guokefeng.cool@163.com).

Wei-Ping Zhu is with the Department of Electrical and Computer Engineering, Concordia University, Montreal, QC H3G1M8, Canada, and also with the College of Telecommunications and Information Engineering, Nanjing University of Posts and Telecommunications, Nanjing 210003, China (e-mail: weiping@ece.concordia.ca).

Digital Object Identifier 10.1109/JPHOT.2021.3098328

performance. To achieve higher data rates in the RF link, the authors of [18] and [19] applied multi-antenna relaying techniques in the mixed RF-FSO network. It should be pointed out that the above-mentioned works assumed perfect channel state information (CSI) available in the RF link. In wireless communication systems, however, the perfect CSI is difficult to obtain due to the moving transceivers and the channel estimation mismatches. Therefore, mixed RF-FSO systems based on imperfect CSI have received increasing attention [20]–[22]. The performance of a mixed RF-FSO system was analyzed in [20] where a moving user communicates with the relay via an RF link. To serve multiple terrestrial users, the authors further proposed a novel user scheduling scheme using imperfect CSI in the mixed FSO-RF SATN [21]. Besides, in [22], the authors studied the outage performance of mixed FSO-RF SATN, and concluded that imperfect CSI in the RF link due to the instability of aerial platform would significantly degrade system performance. However, the pervious works did not analyze or evaluate the negative impact of imperfect CSI.

Motivated by these observations, in this paper we introduce BF in a multiuser mixed RF-FSO SATN to reduce the effect of the instability of aerial platform and the mobility of user. We focus on the uplink transmission of the SATN in which the aerial platform employing multiple antennas serves users through RF links, while communicating with a geosynchronous orbit (GEO) satellite through FSO link based on AF protocol. Specifically, our main contributions are listed as follows:

- We analyze the uplink transmission of a practical satellite-aerial-terrestrial network using mixed RF/FSO communication, where the RF link operates with space division multiple access (SDMA) to connect multiple users and experiences Nakagami-m fading, while the satellite-aerial FSO link experiences more general Málaga turbulent fading with nonzero-boresight pointing error, unlike the Gamma-Gamma atmospheric turbulence with zero-boresight pointing error as considered in [17]–[20]. Moreover, we employ only imperfect CSI, instead of perfect CSI as in [16], [17], [19], of the RF links in our analysis.
- By using the angle-of-arrival (AoA) based imperfect CSI of each user, we formulate an optimal BF problem at the aerial platform to maximize the minimum average signal-to-interference-plus-noise ratio (SINR) of the users. Due to the mathematical intractability of the optimization problem, we first use the discretization method to deal with the uncertainty of imperfect CSI. Then, by using Hölder's and Cauchy-Schwarz's inequalities, we propose an iterative algorithm to obtain the optimal BF vector. Compared to the existing works on SATN that were focused on single-antenna aerial platform [10] or single-user scenarios [12], [18], [22], we consider a more general case.
- Based on the proposed optimum BF scheme and the Nakagami-m fading and general Málaga turbulent fading considered for the RF and FSO links, respectively, we analyze the outage probability (OP) for the considered SATN.
- Simulation results are provided to validate our theoretical analysis of the outage performance of the SATN. It has been shown that pointing errors can significantly degrade the performance, particularly for big values of the normalized beam width. Furthermore, the proposed BF scheme exhibits a good robustness of the aerial platform against imperfect CSI in the RF link as compared to the zero forcing (ZF) BF scheme [20] and non-robust BF scheme.

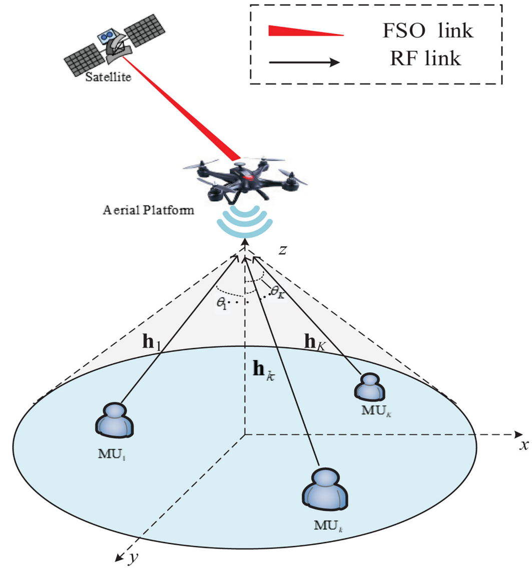

Fig. 1. System model.

Notations: Vectors and matrices are denoted by bold lower-case and upper-case letters, respectively. $\exp(\cdot)$ represents the exponential function; $K_v(\cdot)$ is the modified Bessel function; and $\Gamma(\cdot)$ denotes the gamma function. Besides, $|\cdot|$ is the absolute value of a scalar; $\|\cdot\|$ denotes Euclidean norm of complex vector; $\mathbf{A}^H$ represents the conjugate transpose; $\mathbf{I}_N$ stands for an $N\times N$ identity matrix; $\mathbb{C}^{M\times N}$ complex space of $M\times N$ dimensions; $\mathrm{E}[\cdot]$ denotes the expectation; $\rho\sim Nakagami(m,\Omega)$ denotes that ρ follows Nakagami-m distribution with severity parameter m and average power Ω. Finally, $G_{p,q}^{m,n}[\cdot]$ and $(\cdot)_n$ denote Meijer's G-function and the Pochhammer symbol, respectively [26].

II. System Model

We consider the uplink transmission of a multiuser satellite-aerial-terrestrial network as shown in Fig. 1, where K mobile IoT users (MUs) transmit messages through RF links to a hovering aerial platform, which acts as an AF relay and sends the received messages to the satellite through an FSO link. The aerial platform is equipped with an N-element $(N>K)$ uniform linear array (ULA) to take the advantage of BF, while each MU employs a single antenna.

A. Channel Models

To realistically model the aerial-terrestrial links, we take the path loss and small-scale fading into account. Mathematically, the channel vector of the aerial-terrestrial link between MU_k and the aerial platform can be obtained as

$$\mathbf{h}_k=\ell_k\mathbf{g}_k, \tag{1}$$

where $\ell_k=\frac{1}{2}(20\lg(d_{\mathrm{km}})+20\lg(f_{\mathrm{GHz}})+92.4)[\mathrm{dB}]$ denotes the free path loss of the aerial-terrestrial link [21] with d_{km} being the distance between MU_k and aerial platform in km, and

f_{GHz} the frequency in GHz, and the channel fading vector of aerial-terrestrial link $\mathbf{g}_k$ is given by

$$\mathbf{g}_k = \rho_k \mathbf{a}\left(\theta_k\right), \tag{2}$$

where ρ_k is a Nakagami-m random variable with severity parameter m_k and average power Ω_k, and $\mathbf{a}(\theta_k)$ is the array steering vector, namely,

$$\mathbf{a}\left(\theta_k\right) = \left[1, \exp\left(j2\pi\frac{d_e}{\lambda}\sin\theta_k\right), \ldots, \exp\left(j2\pi\left(N-1\right)\frac{d_e}{\lambda}\sin\theta_k\right)\right], \tag{3}$$

with d_e being the antenna spacing at the aerial platform, λ the carrier wavelength, and θ_k the AoA of the antenna.

The fading channel coefficient of the aerial-satellite link can be expressed as [21]

$$h_{FSO} = \ell_{FSO} h_a h_p, \tag{4}$$

where the path loss ℓ_{FSO} is given by $\ell_{FSO} = \frac{1}{2}(G_t + G_r - Att_{FS} - Att_{Atm} - L_{lenses} - M)[dB]$. The parameters G_t and G_r are the transmitter and receiver gains, respectively, Att_{FS} the free space losses, Att_{Atm} the atmospheric attenuation, L_{lenses} the lenses losses, and M a system margin. In addition, we use Málaga distribution to describe the atmospheric turbulence induced fading h_a, whose probability density function (PDF) is given by [23]

$$f_{h_a}(I) = A\sum_{k=1}^{\beta} a_k I^{\frac{\alpha+k}{2}-1} K_{\alpha-k}\left(2\sqrt{\frac{\alpha\beta I}{g\beta+\Omega'}}\right) \tag{5}$$

with $A \triangleq \frac{2\alpha^{\frac{\alpha}{2}}}{g^{1+\frac{\alpha}{2}}\Gamma(\alpha)}\left(\frac{g\beta}{g\beta+\Omega'}\right)^{\frac{\alpha}{2}+\beta}$, and $a_k \triangleq \binom{\beta-1}{k-1}\frac{(g\beta+\Omega')^{1-\frac{k}{2}}}{(k-1)!}\left(\frac{\Omega'}{g}\right)^{k-1}\left(\frac{\alpha}{\beta}\right)^{\frac{k}{2}}$, where α represents a positive parameter related to the effective number of large-scale cells of the scattering process, $\beta \in \mathbb{N}$ denotes the amount of fading parameter, and $g = 2b_0(1-\rho)$. Here, $2b_0$ denotes the average power of the total scatter components, and the parameter $\rho \in [0,1]$ defines the amount of the scattering power coupled to the LoS component $\Omega' = \Omega + 2b_0\rho + 2\sqrt{2b_0\Omega\rho}\cos(\phi_A - \phi_B)$ where Ω is the average power of the LoS component, ϕ_A the deterministic angles for the LoS component, and ϕ_B the coupled-to-LoS scatter terms.

In (4), h_p stands for the non-zero boresight pointing error. Due to the fact that the aerial platform is instable and unaligned with satellite, the pointing errors should be considered. Thus, we adopt a general and comprehensive model, which integrates the effect of beam width, detector size, different jitters for the elevation and the horizontal displacement, and the effect of nonzero boresight error. The attenuation due to geometric spread and pointing errors can be approximated as [24]

$$h_p\left(r; z\right) \approx A_0 \exp\left(-\frac{2r^2}{\omega_{zeq}^2}\right), \tag{6}$$

where $r \geq 0$ denotes the radial displacement at the receiver plane, and ω_{zeq} is the equivalent beam radius defined as $\omega_{zeq} = \omega_z^2\frac{\sqrt{\pi}A_0}{2\nu\exp(-\nu^2)}$, with ω_z being beam waist at the distance z and $A_0 = [\mathrm{erf}(\nu)]^2, \nu = \sqrt{\frac{\pi}{2}}\frac{a}{\omega_z}$ is the detection radius of the FSO receiver. For simplicity, the beam width ω_z can be approximated by $\omega_z = \varpi z$ where ϖ is the transmit divergence angle defining

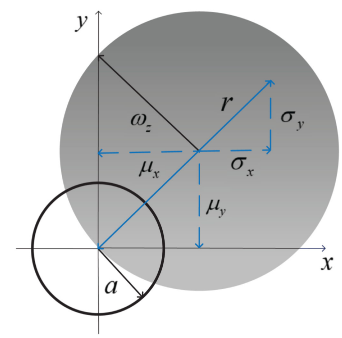

Fig. 2. Beam footprint with generalized pointing errors on the receiver aperture plane.

the increase in beam radius with a link distance. As shown in Fig. 2, x and y represent the horizontal displacement and the elevation, respectively. The radial displacement can be further represented as $r^2 = r_x^2 + r_y^2$. We consider a nonzero boresight error in addition to the random jitters, and model each component as nonzero mean Gaussian random variables, i.e., $r_x \sim N(\mu_x, \sigma_x^2)$, $r_y \sim N(\mu_y, \sigma_y^2)$. Thus, the radial displacement r follows the Beckmann distribution [24]

$$f_r\left(r\right) = \frac{r}{2\pi\sigma_x\sigma_y}\int_0^{2\pi} \exp\left\{-\frac{\left(r\cos\varpi-\mu_x\right)^2}{2\sigma_x^2} - \frac{\left(r\sin\varpi-\mu_y\right)^2}{2\sigma_y^2}\right\} d\varpi. \tag{7}$$

Since there is no closed-form expression for the above Beckmann distribution, we use the approximation of the Beckmann distribution presented in [24], which is given by

$$f_r(r) = \frac{r}{\sigma_{\mathrm{mod}}^2}\exp\left(-\frac{r^2}{2\sigma_{\mathrm{mod}}^2}\right) \tag{8}$$

where σ_{mod} is the misalignment parameter related to the two displacement components, which can be expressed as

$$\sigma_{\mathrm{mod}}^2 = \sqrt[3]{\frac{3\mu_x^2\sigma_x^4 + 3\mu_y^2\sigma_y^4 + \sigma_x^6 + \sigma_y^6}{2}}. \tag{9}$$

Substituting (6) into (8), we obtain the PDF of h_P as

$$f_{h_p}(I) = \frac{\tau_{\mathrm{mod}}^2}{A_{\mathrm{mod}}^{\tau_{\mathrm{mod}}^2}} I^{\tau_{\mathrm{mod}}^2 - 1}, 0 \leq I \leq A_{\mathrm{mod}}, \tag{10}$$

where $\varphi_{\mathrm{mod}} = \omega_{eq}/2\sigma_{\mathrm{mod}}$ and A_{mod} is given by

$$A_{\mathrm{mod}} = A_0\exp\left(\frac{1}{\varphi_{\mathrm{mod}}^2} - \frac{1}{2\varphi_x^2} - \frac{1}{2\varphi_y^2} - \frac{\mu_x^2}{2\sigma_x^2\varphi_x^2} - \frac{\mu_y^2}{2\sigma_y^2\varphi_y^2}\right) \tag{11}$$

with $\varphi_x = \frac{\omega_{eq}}{2\sigma_x}$ and $\varphi_x = \frac{\omega_{eq}}{2\sigma_y}$.

When $\mu_x = \mu_y = 0, \sigma_x = \sigma_y = \sigma_s$, the non-zero boresight pointing error reduces to the special case of zero boresight error [21], [22]. Therefore, we can extend the previous system model to a more general case.

B. Signal Model

The uplink transmission from the multiple mobile users to the satellite can be divided into two phases. In the first phase, all MUs are connected through RF access links to the aerial platform simultaneously using SDMA. Thus, the received signal at the aerial platform from MU_k is given by

$$y_{R,k}(t) = \mathbf{w}_k^H \mathbf{h}_k \sqrt{P_k} x_k(t) + \mathbf{w}_k^H \sum_{i=1, i\neq k}^{K} \mathbf{h}_i \sqrt{P_i} x_i(t) + \mathbf{w}_k^H \mathbf{n}_R(t), \quad (12)$$

where P_k and $x_k(t)$ represent the transmit power and message at the MU_k, respectively, $\mathbf{h}_k \in \mathbb{C}^{K\times 1}$ is the channel vector between MU_k and the aerial platform, $\mathbf{w}_k \in \mathbb{C}^{N\times 1}$ is unit-norm BF vector of MU_k satisfying $\|\mathbf{w}_k\| = 1$, and $\mathbf{n}_R(t)$ is the additive white Gaussian noise (AWGN) satisfying $\mathbf{n}_R(t) \sim \mathbb{CN}(\mathbf{0}, \sigma_R^2 \mathbf{I}_N)$.

For the second phase, considering that the aerial platform is power-limited, the lower-complexity AF protocol is used in this work. Thus, the received RF signal $y_{R,k}(t)$ is first amplified with a fixed gain G_k, as given by

$$G_k = 1/\mathrm{E}\left[\sqrt{\sum_{i=1}^{K} P_i \mathbf{w}_k^H \mathbf{h}_i \mathbf{h}_i^H \mathbf{w}_k + \sigma_R^2}\right], \quad (13)$$

and then the RF signals are converted into an optical signal using the subcarrier intensity modulation before being transmitted to the satellite [16]. Finally, the satellite filters out the direct current component, and extracts the received signal from MU_k as

$$\begin{aligned} y_{D,k}(t) &= \sqrt{P_R} G_k \zeta h_{FSO} \left(\mathbf{w}_k^H \mathbf{h}_k \sqrt{P_k} x_k(t) \right. \\ &\left. + \mathbf{w}_k^H \sum_{i=1, i\neq k}^{K} \mathbf{h}_i \sqrt{P_i} x_i(t) + \mathbf{w}_k^H \mathbf{n}_r(t) \right) + n_D(t) \end{aligned} \quad (14)$$

where P_R denotes the aerial platform transmit power, ζ is the electrical-to-optical conversion coefficient, and $n_D(t)$ denotes AWGN with zero mean and variance σ_D^2. Thus, the end-to-end SINR of MU_k signal at the satellite is given by

$$\begin{aligned} \gamma_{D,k} &= \frac{P_R G_k^2 \zeta^2 |h_{FSO}|^2 P_k \left|\mathbf{w}_k^H \mathbf{h}_k\right|^2}{P_R G_k^2 \zeta^2 |h_{FSO}|^2 \left(\sum_{i=1, i\neq k}^{K} P_i \left|\mathbf{w}_k^H \mathbf{h}_i\right|^2 + \sigma_R^2 \right) + \sigma_D^2} \\ &\triangleq \frac{\gamma_{k,k}\gamma_{FSO}}{\gamma_{FSO}\left(\gamma_{k,I}+1\right) + C_k} \end{aligned} \quad (15)$$

where $\gamma_{k,i} = \frac{P_i}{\sigma_R^2}|\mathbf{w}_k^H \mathbf{h}_i|^2$, $\gamma_{FSO} = \frac{P_S \zeta^2}{\sigma_D^2}|h_{FSO}|^2$, $\gamma_{k,I} = \sum_{i=1\&i\neq k}^{K} \gamma_{k,i}$, and $C_k = \mathrm{E}[1 + \gamma_{k,k} + \gamma_{k,I}]$.

III. Proposed BF Scheme

To ensure the quality of service for each user, we aim at maximizing the minimum average SINR through solving the following BF optimization problem

$$\begin{aligned} \max_{\mathbf{w}_1,\ldots,\mathbf{w}_K} \min_{k} \quad & \mathrm{E}\left[\gamma_{D,k}\right] \\ \text{s.}t. \quad & ||\mathbf{w}_k|| = 1, \forall k = 1,\ldots,K. \end{aligned} \quad (16)$$

Unlike previous works, we consider the instability of aerial platform and the mobility of user in our BF design. We assume that the RF channel is within given uncertainty sets, which are available at the aerial platform, and can be expressed as [25]

$$\Delta_l = \left\{\mathbf{h}_l | \theta_l \in [\theta_{l,L}, \theta_{l,U}]\right\}, l \in \{i,k\}, \quad (17)$$

where $\theta_{l,L}$ and $\theta_{l,U}$ denote the lower and upper bounds of AoA, respectively. Substituting (17) into (16), we can reformulate the original BF problem as

$$\begin{aligned} \max_{\mathbf{w}_1,\ldots,\mathbf{w}_K} \min_{k} \min_{\mathbf{h}_l\in\Delta_l} \quad & \mathrm{E}\left[\gamma_{D,k}\right] \\ \text{s.}t. \quad & ||\mathbf{w}_k|| = 1, \forall k = 1,\ldots,K. \end{aligned} \quad (18)$$

Since the optimization problem is mathematically intractable, we use Mullen's inequality to approximate the objective function $\mathrm{E}[\gamma_{D,k}]$ as

$$\begin{aligned} \mathrm{E}\left[\gamma_{\mathrm{D,k}}\right] &\approx \frac{\mathrm{E}\left[\gamma_{k,k}\right]\mathrm{E}\left[\gamma_{FSO}\right]}{\mathrm{E}\left[\gamma_{FSO}\right]\mathrm{E}\left[\gamma_{k,I}+1\right] + \mathrm{E}\left[\gamma_{k,k}\right] + \mathrm{E}\left[\gamma_{k,I}+1\right]} \\ &= \frac{\left(\mathrm{E}\left[\gamma_{k,k}\right]/\mathrm{E}\left[\gamma_{k,I}+1\right]\right)\mathrm{E}\left[\gamma_{FSO}\right]}{\mathrm{E}\left[\gamma_{FSO}\right] + \left(\mathrm{E}\left[\gamma_{k,k}\right]/\mathrm{E}\left[\gamma_{k,I}+1\right]\right) + 1}. \end{aligned} \quad (19)$$

It can be shown that $\mathrm{E}[\gamma_{FSO}]$ is not affected by the BF vectors $\mathbf{w}_k$, and it monotonically increases with $\mathrm{E}[\gamma_{k,k}]/\mathrm{E}[\gamma_{k,I}+1]$ and $\mathrm{E}[\gamma_{FSO}]$. The optimization problem can be further expressed as

$$\begin{aligned} \max_{\mathbf{w}_1,\ldots,\mathbf{w}_K} \min_{k} \min_{\mathbf{h}_l\in\Delta_l} & \frac{\mathrm{E}[\gamma_{k,k}]}{\mathrm{E}\left[\gamma_{k,I}+1\right]} \\ &= \frac{\mathrm{E}\left[\bar{\gamma}_k \mathbf{w}_k^H \mathbf{h}_k \mathbf{h}_k^H \mathbf{w}_k\right]}{\mathrm{E}\left[\sum_{i=1\&i\neq k}^{K} \bar{\gamma}_i \mathbf{w}_k^H \mathbf{h}_i \mathbf{h}_i^H \mathbf{w}_k + 1\right]} \\ \text{s.}t. \; & ||\mathbf{w}_k|| = 1, \forall k = 1,\ldots,K, \end{aligned} \quad (20)$$

where $\bar{\gamma}_l = \frac{P_l \ell_l^2}{\sigma_R^2}$. Because $\mathbf{w}_k (\forall k = 1,\ldots,K)$ is mutually independent, the optimization problem (20) can be decomposed into K independent sub-problems as

$$\begin{aligned} \max_{\mathbf{w}_k} \min_{\mathbf{h}_l\in\Delta_l} \quad & \frac{\bar{\gamma}_k \mathbf{w}_k^H \mathrm{E}\left[\mathbf{h}_k \mathbf{h}_k^H\right] \mathbf{w}_k}{\sum_{i=1\&i\neq k}^{K} \bar{\gamma}_i \mathbf{w}_k^H \mathrm{E}\left[\mathbf{h}_i \mathbf{h}_i^H\right] \mathbf{w}_k + 1} \\ \text{s.}t. \quad & ||\mathbf{w}_k|| = 1, \end{aligned} \quad (21)$$

where $\mathrm{E}[\mathbf{h}_l \mathbf{h}_l^H] = \mathrm{E}[\rho_l^2]\mathbf{a}(\theta_l)\mathbf{a}(\theta_l)^H = \Omega_l \mathbf{H}_l$ with $\Omega_l = \mathrm{E}[|\rho_l|^2]$ and $\mathbf{H}_l = \mathbf{a}(\theta_l)\mathbf{a}(\theta_l)^H$. It can be found that the objective function includes AoA uncertainty region Δ_l, which makes the optimization still difficult to solve. To address this problem, we discretize the channel uncertainty region in (21). Specifically, we first divide uniformly the uncertain region Δ_l as

$$\theta_l^{(j)} = \theta_{l,L} + j\Delta\theta_l, j = 0,\ldots,M_l, \quad (22)$$

where $\Delta\theta_l = (\theta_{l,U} - \theta_{l,L})/M_l$, and $M_l \geq N$ represents the number of samples. Then, we define Ψ_l as [25]

$$\Psi_l = \left\{ \sum_{j=1}^{M_l} \mu_{l,j} \mathbf{H}_{l,j} \middle| \sum_{j=1}^{M_l} \mu_{l,j} = 1,\ \mu_{l,j} 0 \right\}, \quad \forall l \in \{1,\ldots,K\}, \quad (23)$$

where $\mathbf{H}_{l,j} \triangleq \mathbf{a}(\theta_l^{(j)})\mathbf{a}(\theta_l^{(j)})^H$, and $\mu_{l,j}$ denotes the weighted coefficient. Furthermore, the optimization problem (21) can be rewritten as

$$\begin{aligned} \min_{\{\mu_{k,j},\mu_{i,j}\}} \max_{\mathbf{w}_k} \quad & \frac{\mathbf{w}_k^H \left(\bar{\gamma}_k \Omega_k \sum_{j=1}^{M_k} \mu_{k,j} \mathbf{H}_{k,j} \right) \mathbf{w}_k}{\mathbf{w}_k^H \left(\sum_{i=1\&i\neq k}^{K} \sum_{j=1}^{M_i} \bar{\gamma}_i \Omega_i \mu_{i,j} \mathbf{H}_{i,j} + \mathbf{I} \right) \mathbf{w}_k} \\ s.t. \quad & ||\mathbf{w}_k|| = 1. \end{aligned} \quad (24)$$

Note that (24) is still mathematically intractable. We now propose an iterative algorithm to obtain the BF vector. First, for given $\mu_{k,j}$ and $\mu_{i,j}$, using generalized Rayleigh quotient, we obtain the BF vector $\mathbf{w}_k$ as

$$\mathbf{w}_k = \left\{ \mathrm{eig}\left(\bar{\gamma}_k \Omega_k \sum_{j=1}^{M_k} \mu_{k,j} \mathbf{H}_{k,j}, \sum_{i=1\&i\neq k}^{K} \sum_{j=1}^{M_i} \bar{\gamma}_i \Omega_i \mu_{i,j} \mathbf{H}_{i,j} + \mathbf{I} \right) \right\} \tag{25}$$

where $\mathrm{eig}(\mathbf{A}, \mathbf{B})$ represents the normalized eigenvector corresponding to the largest generalized eigenvalue of the matrix $\mathbf{B}^{-1}\mathbf{A}$. Then, the value of $\mu_{k,j}$, $\mu_{i,j}$ are used to minimize the objective function in (24). By utilizing Hölder's inequality, we obtain

$$\sum_{j=1}^{M_k} \mu_{k,j} \mathbf{w}_k^H \mathbf{H}_{k,j} \mathbf{w}_k \geq \left(\sum_{j=1}^{M_k} (\mu_{k,j})^{\frac{1}{2}} \right)^2 \left(\sum_{j=1}^{M_k} \left(\mathbf{w}_k^H \mathbf{H}_{k,j} \mathbf{w}_k \right)^{-1} \right)^{-1}. \tag{26}$$

The equality holds true only if $\frac{(\mu_{k,j})^{\frac{1}{2}}}{\sum_{j=1}^{M_k} (\mu_{k,j})^{\frac{1}{2}}} = \frac{(\mathbf{w}_k^H \mathbf{H}_{k,j} \mathbf{w}_k)^{-1}}{\sum_{j=1}^{M_k} (\mathbf{w}_k^H \mathbf{H}_{k,j} \mathbf{w}_k)^{-1}} = A_{k,j}, \forall j$. To minimize the numerator of the objective function in (24), $\mu_{k,j}$ is given by

$$\mu_{k,j} = \frac{(A_{k,j})^2}{\sum_{j=1}^{M_k} (A_{k,j})^2}. \tag{27}$$

By applying Cauchy-Schwarz's inequality, we obtain

$$\left(\sum_{j=1}^{M_i} \mu_{i,j} \mathbf{w}_k^H \mathbf{H}_{i,j} \mathbf{w}_k \right)^2 \leq \left(\sum_{j=1}^{M_i} \mu_{i,j}^2 \right) \left(\sum_{j=1}^{M_i} \left(\mathbf{w}_k^H \mathbf{H}_{i,j} \mathbf{w}_k \right)^2 \right). \tag{28}$$

The equality holds true only if $\frac{\mu_{i,1}}{\mathbf{w}_k^H \mathbf{H}_{i,1} \mathbf{w}_k} = \frac{\mu_{i,2}}{\mathbf{w}_k^H \mathbf{H}_{i,2} \mathbf{w}_k} = \cdots = \frac{\mu_{i,M_i}}{\mathbf{w}_k^H \mathbf{H}_{i,M_i} \mathbf{w}_k}$. Furthermore, to maximize the denominator of objective function (24), $\mu_{i,j}$ is given by

$$\mu_{i,j} = \frac{\mathbf{w}_k^H \mathbf{H}_{i,j} \mathbf{w}_k}{\sum_{j=1}^{M_i} \mathbf{w}_k^H \mathbf{H}_{i,j} \mathbf{w}_k}. \tag{29}$$

Substituting (27) and (29) into (25), we compute and update BF vector $\mathbf{w}_k$. Moreover, $\mu_{k,j}$, $\mu_{i,j}$, and $\mathbf{w}_k$ are operated iteratively until γ_k no longer increases, yielding the optimal BF vector $\mathbf{w}_k^*$. The proposed iterative algorithm to compute the robust BF vectors is summarized in Algorithm 1.

IV. Outage Performance

In this section, we focus on the outage performance of the considered SATN with the proposed BF scheme. The outage probability of MU_k is defined as the probability that $\gamma_{D,k}$ falls below a certain threshold γ_{th}, i.e.,

$$P_{out,k}(\gamma_{th}) = \Pr\{\gamma_{D,k} < \gamma_{th}\}. \tag{30}$$

Algorithm 1: The Proposed Iterative Algorithm.

1: Initialize $m = 0$;
2: Let θ_l be uniformly distributed in $[\theta_{l,L}, \theta_{l,U}]$, and further construct $\mathbf{H}_{l,j}, l \in \{i,k\}, j \in \{1,\ldots,M_l\}$;
3: Let $\gamma_k = \frac{\mathrm{E}[\gamma_{k,k}]}{\mathrm{E}[\gamma_{k,I}+1]}$;
4: Set $\mu_{k,j}^0 = \frac{1}{M_k}, \mu_{i,j}^0 = \frac{1}{M_i}$ and the convergence tolerance $\delta > 0$;
5: Calculate $\mathbf{w}_k^0$and γ_k^0 through (25);
6: **while** $|\gamma_k^m - \gamma_k^{m-1}| > \delta$ **do**
7: $m := m+1$;
8: Compute the coefficient : $\frac{(\mu_{k,j})^{\frac{1}{2}}}{\sum_{j=1}^{M_k} (\mu_{k,j})^{\frac{1}{2}}} = \frac{((\mathbf{w}_k^{m-1})^H \mathbf{H}_{k,j} \mathbf{w}_k^{m-1})^{-1}}{\sum_{j=1}^{M_k} ((\mathbf{w}_k^{m-1})^H \mathbf{H}_{k,j} \mathbf{w}_k^{m-1})^{-1}}, \forall j$;
9: Update $\mu_{k,j}^m := \frac{(A_{k,j}^m)^2}{\sum_{j=1}^{M_k} (A_{k,j}^m)^2}$, $\mu_{i,j}^m := \frac{(\mathbf{w}_k^{m-1})^H \mathbf{H}_{i,j} \mathbf{w}_k^{m-1}}{\sum_{j=1}^{M_i} (\mathbf{w}_k^{m-1})^H \mathbf{H}_{i,j} \mathbf{w}_k^{m-1}}$;
10: Compute $\mathbf{w}_k^m$ and γ_k^m using (25);
11: **end while**
12: Substitute $\{\mu_{k,j}^m\}$ and $\{\mu_{i,j}^m\}$ into (25) to obtain $\mathbf{w}_k^*$.

Substituting (15) into (30) gives

$$P_{out,k}(\gamma_{th}) = \Pr\left\{ \frac{\gamma_{k,k}\gamma_{FSO}}{\gamma_{FSO}(\gamma_{k,I}+1) + C_k} \leqslant \gamma_{th} \right\} = \int_0^\infty \int_0^\infty \Pr\left\{ \gamma_{k,k} \leqslant \gamma_{th}\gamma_{k,I} + \gamma_{th} + \frac{C_k \gamma_{th}}{\gamma_{FSO}} \right\} f_{\gamma_{FSO}}(\gamma_{FSO}) f_{\gamma_{k,I}}(\gamma_{k,I}) \, d\gamma_{FSO} d\gamma_{k,I} \tag{31}$$

To calculate the integral, we first derive the PDFs of γ_{FSO} and $\gamma_{k,I}$, and the cumulative distribution function (CDF) of $\gamma_{k,k}$. The joint distribution of $h_{FSO} = \ell_{FSO} h_a h_p$ is derived by

$$f_{h_{FSO}}(I) = \int_{I/(\ell_{FSO} A_{\mathrm{mod}})}^{\infty} f_{h_a}(I_a) f_{I|h_a}(I|I_a) \, dI_a = \int_{I/(\ell_{FSO} A_{\mathrm{mod}})}^{\infty} f_{h_a}(I_a) \frac{I}{I_a \ell_{FSO}} f_{h_p}\left(\frac{I}{I_a \ell_{FSO}} \right) dI_a. \tag{32}$$

Applying simple random variable substitution, we obtain the PDF of $\gamma_{FSO} = \frac{P_S \zeta^2}{\sigma_D^2} |h_{FSO}|^2$ as

$$f_{\gamma_{FSO}}(I) = \frac{\tau_{\mathrm{mod}}^2 A_{\mathrm{mod}}}{4I} \sum_{n=1}^{\beta} a_n \left(\frac{\alpha\beta}{g\beta + \Omega'} \right)^{-\frac{\alpha+n}{2}} \times G_{1,3}^{3,0}\left[\frac{\alpha\beta}{(g\beta + \Omega') A_{\mathrm{mod}}} \sqrt{\frac{I}{\bar{\gamma}_{FSO}}} \middle| \begin{matrix} \tau_{\mathrm{mod}}^2 + 1 \\ \tau_{\mathrm{mod}}^2, \alpha, n \end{matrix} \right] \tag{33}$$

where $\bar{\gamma}_{FSO} = \frac{P_S \zeta^2}{\sigma_D^2}$. Next, we focus on the CDF of $\gamma_{k,k}$ and the PDF of $\gamma_{k,I}$. Since $\mathbf{w}_k^*$ is obtained by the robust BF scheme, $\gamma_{k,i}$ can be denoted as

$$\gamma_{k,i} = \bar{\gamma}_i \left| (\mathbf{w}_k^*)^H \mathbf{h}_i \right|^2 = \bar{\gamma}_i \left| (\mathbf{w}_k^*)^H \mathbf{a}_i(\theta_i) \right|^2 \rho_i^2. \tag{34}$$

Note that $|(\mathbf{w}_k^*)^H \mathbf{a}_i(\theta)|^2$ in (34) is a constant, and $|\rho_i|$ follows $Nakagami(m_i, \Omega_i)$ distribution. Thus, the PDF of $\gamma_{k,i}$ can be denoted as

$$f_{\gamma_{k,i}}(x) = \left(\frac{\eta_{k,i}}{\bar{\gamma}_i}\right)^{m_i} \frac{x^{m_i-1}}{\Gamma(m_i)} \exp\left(-\frac{\eta_{k,i}x}{\bar{\gamma}_i}\right), \quad (35)$$

where $\eta_{k,i} = m_i/(\omega_{k,i}\Omega_i)$ with $\omega_{k,i} = |(\mathbf{w}_k^*)^H \mathbf{a}_i(\theta)|^2$. In addition, resorting to Eq. (3.351.1) in [26] and using (35), the CDF of $\gamma_{k,i}$ is given by

$$F_{\gamma_{k,i}}(x) = 1 - \exp\left(-\frac{\eta_{k,i}x}{\bar{\gamma}_i}\right) \sum_{p=0}^{m_i-1} \frac{1}{p!}\left(\frac{\eta_{k,i}x}{\bar{\gamma}_i}\right)^p. \quad (36)$$

According to (35), the Laplace transform of $\gamma_{k,i}$ can be calculated as

$$\begin{aligned}\psi_{\gamma_{k,i}}(s) &= \mathrm{E}\left[\exp\left(-s\gamma_{k,i}\right)\right] = \int_0^\infty \exp\left(-sx\right) f_{\gamma_{k,i}}(x)dx \\ &= \left(\frac{\eta_{k,i}}{\bar{\gamma}_i}\right)^{m_i} \frac{1}{\Gamma(m_i)} \int_0^\infty x^{m_i-1} \exp\left(-sx - \frac{\eta_{k,i}x}{\bar{\gamma}_i}\right)dx.\end{aligned} \quad (37)$$

From [26, Eq. (3.351.3)], we further have

$$\psi_{\gamma_{k,i}}(s) = \left(\frac{\eta_{k,i}}{\bar{\gamma}_i}\right)^{m_i} \left(\frac{\eta_{k,i}}{\bar{\gamma}_i} + s\right)^{-m_i}. \quad (38)$$

Then, the Laplace transform of $\gamma_{k,I}$ can be calculated as

$$\begin{aligned}\psi_{\gamma_{k,I}}(s) &= \left[\prod_{i=1\&i\neq k}^{K} \exp\left(-s\gamma_{k,i}\right)\right] = \prod_{i=1\&i\neq k}^{K} \psi_{\gamma_{k,i}}(s) \\ &= \left(\prod_{i=1\&i\neq k}^{K} \left(\frac{\eta_{k,i}}{\bar{\gamma}_i}\right)^{m_i}\right) \left(\prod_{i=1\&i\neq k}^{K} \left(\frac{\eta_{k,i}}{\bar{\gamma}_i} + s\right)^{-m_i}\right).\end{aligned} \quad (39)$$

According to the inverse Laplace transform, the PDF of $\gamma_{k,I}$ can be expressed as

$$\begin{aligned}f_{\gamma_{k,I}}(x) &= \left(\prod_{i=1\&\, i\neq k}^{K} \left(\frac{\eta_{k,i}}{\bar{\gamma}_i}\right)^{m_i}\right) \\ &\times \sum_{i=1\&\, i\neq k}^{K} \sum_{l=1}^{m_i} A_{i,l}\left(-\frac{\eta_{k,i}}{\bar{\gamma}_i}\right) x^{l-1} \exp\left(-\frac{\eta_{k,i}x}{\bar{\gamma}_i}\right)\end{aligned} \quad (40)$$

where $A_{i,l}(s) = \frac{1}{\Gamma(m_i-l+1)\Gamma(l)} \frac{d^{m_i-l}}{s^{m_i-l}} [\prod_{j=1\&j\neq k\neq i}^{K} (s + \frac{\eta_{k,j}}{\bar{\gamma}_j})^{-m_j}]$. Further, plugging the PDF of γ_{FSO} and the CDF of $\gamma_{k,k}$ into $P_{out,k}(\gamma_{th})$, we obtain

$$\begin{aligned}&P_{out,k}(\gamma_{th}) \\ &= 1 - \mathrm{E}_{\gamma_{k,I}}\left[\int_0^\infty \frac{\tau_{\mathrm{mod}}^2 A_{\mathrm{mod}}}{4\gamma_{FSO}} \sum_{n=1}^{\beta} a_n \left(\frac{\alpha\beta}{g\beta+\Omega'}\right)^{-\frac{\alpha+n}{2}}\right. \\ &G_{1,3}^{3,0}\left[\frac{\alpha\beta}{(g\beta+\Omega')A_{\mathrm{mod}}}\sqrt{\frac{\gamma_{FSO}}{\bar{\gamma}_{FSO}}}\,\middle|\, \begin{matrix}\tau_{\mathrm{mod}}^2+1\\ \tau_{\mathrm{mod}}^2, \alpha, n\end{matrix}\right] \\ &\times \exp\left(-\frac{\eta_{k,k}\gamma_{th}}{\bar{\gamma}_k}\left(\gamma_{k,I}+1+\frac{C_k}{\gamma_{FSO}}\right)\right) \\ &\left.\sum_{p=0}^{m_i-1} \frac{1}{p!}\left(\frac{\eta_{k,k}\gamma_{th}}{\bar{\gamma}_k}\left(\gamma_{k,I}+1+\frac{C_k}{\gamma_{FSO}}\right)\right)^p d\gamma_{FSO}\right]\end{aligned} \quad (41)$$

In (41), C_k can be calculated by

$$\begin{aligned}C_k &= \mathrm{E}\left[1+\gamma_{k,I}+\gamma_{k,k}\right] \\ &= 1 + \left(\prod_{i=1}^{K}\left(\frac{\eta_{k,i}}{\bar{\gamma}_i}\right)^{m_i}\right) \sum_{i=1}^{K}\sum_{l=1}^{m_i} A_{i,l}\left(-\frac{\eta_{k,i}}{\bar{\gamma}_i}\right) \\ &\int_0^\infty x^l \exp\left(-\frac{\eta_{k,i}x}{\bar{\gamma}_i}\right)dx,\end{aligned} \quad (42)$$

which leads to [26, Eq.(3.351.3)]

$$C_k = 1 + \left(\prod_{i=1}^{K}\left(\frac{\eta_{k,i}}{\bar{\gamma}_i}\right)^{m_i}\right) \sum_{i=1}^{K}\sum_{l=1}^{m_i} A_{i,l}\left(-\frac{\eta_{k,i}}{\bar{\gamma}_i}\right) l! \left(\frac{\eta_{k,i}}{\bar{\gamma}_i}\right)^{-l-1}. \quad (43)$$

Utilizing the binomial expansion in [26, Eq. (1.111)], $P_{out,k}(\gamma_{th})$ can be further written as (44), shown at the bottom of the page. With the help of Eq. (8.4.3.2) in [27], $\exp(-\frac{\eta_{k,k}\gamma_{th}C_k}{\bar{\gamma}_k\gamma_{FSO}})$ can be written as

$$\exp\left(-\frac{\eta_{k,k}\gamma_{th}C_k}{\bar{\gamma}_k\gamma_{FSO}}\right) = G_{1,0}^{0,1}\left[\frac{\bar{\gamma}_k\gamma_{FSO}}{\eta_{k,k}\gamma_{th}C_k}\,\middle|\, 1\right]. \quad (45)$$

Utilizing Eq. (07.34.21.0013.01) in [28] to compute I_1 in (44) gives

$$\begin{aligned}I_1 &= \frac{2^{\alpha+n-1}}{2\pi}\left(\frac{\bar{\gamma}_k}{\eta_{k,k}\gamma_{th}C_k}\right)^q G_{2,7}^{7,0}\left[\left(\frac{\alpha\beta}{4\sqrt{\bar{\gamma}_{FSO}}(g\beta+\Omega')A_{\mathrm{mod}}}\right)^2\right. \\ &\left.\frac{\eta_{k,k}\gamma_{th}C_k}{\bar{\gamma}_k}\,\middle|\, \begin{matrix}\frac{\tau_{\mathrm{mod}}^2+1}{2}, \frac{\tau_{\mathrm{mod}}^2+2}{2} \\ \frac{\tau_{\mathrm{mod}}^2}{2}, \frac{\tau_{\mathrm{mod}}^2+1}{2}, \frac{\alpha}{2}, \frac{\alpha+1}{2}, \frac{n}{2}, \frac{n+1}{2}, q\end{matrix}\right].\end{aligned} \quad (46)$$

Finally, substituting I_1 and the PDF of $\gamma_{k,I}$ into (44), and using [26, Eq. (3.351.3)], $P_{out,k}(\gamma_{th})$ can be re-expressed as

$$\begin{aligned}P_{out,k}(\gamma_{th}) &= 1 - \frac{\tau_{\mathrm{mod}}^2 A_{\mathrm{mod}}}{4} \sum_{n=1}^{\beta} a_n \left(\frac{\alpha\beta}{g\beta+\Omega'}\right)^{-\frac{\alpha+n}{2}} \\ &\exp\left(-\frac{\eta_{k,k}\gamma_{th}}{\bar{\gamma}_k}\right) \sum_{p=0}^{m_i-1}\frac{1}{p!}\left(\frac{\eta_{k,k}\gamma_{th}}{\bar{\gamma}_k}\right)^p \sum_{q=0}^{p}\binom{p}{q} C_k^q I_1 \\ &\times \sum_{u=0}^{p-q}\binom{p-q}{u}\left(\prod_{i=1\&i\neq k}^{K}\left(\frac{\eta_{k,i}}{\bar{\gamma}_i}\right)^{m_i}\right)\sum_{i=1\&i\neq k}^{K} \\ &\sum_{l=1}^{m_i} A_{i,l}\left(-\frac{\eta_{k,i}}{\bar{\gamma}_i}\right)(u+l-1)!\left(\frac{\eta_{k,i}}{\bar{\gamma}_i}+\frac{\eta_{k,k}\gamma_{th}}{\bar{\gamma}_k}\right)^{-u-l}.\end{aligned} \quad (47)$$

$$\begin{aligned}P_{out,k}(\gamma_{th}) &= 1 - \mathrm{E}_{\gamma_{k,I}}\left[\frac{\tau_{\mathrm{mod}}^2 A_{\mathrm{mod}}}{4}\sum_{n=1}^{\beta} a_n\left(\frac{\alpha\beta}{g\beta+\Omega'}\right)^{-\frac{\alpha+n}{2}} \exp\left(-\frac{\eta_{k,k}\gamma_{th}}{\bar{\gamma}_k}(\gamma_{k,I}+1)\right)\sum_{p=0}^{m_i-1}\frac{1}{p!}\left(\frac{\eta_{k,k}\gamma_{th}}{\bar{\gamma}_k}\right)^p\right. \\ &\left.\times\sum_{q=0}^{p}\binom{p}{q}C_k^q\sum_{u=0}^{p-q}\binom{p-q}{u}\gamma_{k,I}^u \underbrace{\int_0^\infty \gamma_{FSO}^{-q-1} G_{1,3}^{3,0}\left[\frac{\alpha\beta}{(g\beta+\Omega')A_{\mathrm{mod}}}\sqrt{\frac{\gamma_{FSO}}{\bar{\gamma}_{FSO}}}\,\middle|\,\begin{matrix}\tau_{\mathrm{mod}}^2+1\\ \tau_{\mathrm{mod}}^2,\alpha,n\end{matrix}\right]\exp\left(-\frac{\eta_{k,k}\gamma_{th}C_k}{\bar{\gamma}_k\gamma_{FSO}}\right)d\gamma_{FSO}}_{I_1}\right]\end{aligned} \quad (44)$$

TABLE I
MAIN SIMULATION PARAMETERS

Parameters	Values
Height of Satellite	36000km
Height of aerial platform	10km
Number of users	$K = 6$
Number of antennas	$N = 16$
Wavelength of the laser	1550nm
Carrier frequency of RF links	1900MHz
Electrical-to-optical conversion coefficient	$\zeta = 1$

It is worth noting that when the FSO link parameters are set as $\rho = 1$, $g = 0$, and $\Omega' = 1$ in the scenario of single user (i.e., K=1) and single antenna at the aerial platform, (47) reduces to a similar expression for OP as [17, eq. (18)]. Thus, we have obtained a more general OP expression.

V. NUMERICAL RESULTS

In this section, we present numerical results to validate the performance analysis and the superiority of the proposed BF scheme. We define the Málaga turbulent channel fading parameters of the FSO link as α= 10.53 and $\beta = 10$. Some other FSO link parameters used in our simulation are set as $\Omega = 1.3265$, $b_0 = 0.1079$, $\rho = 0.596$, and $\phi_A - \phi_B = \pi/2$. Meanwhile, all the MUs are uniformly distributed in a circular area, and the AoA uncertainty is calculated as $\Delta = \theta_{l,U} - \theta_{l,L}$. For analytical tractability, we suppose all the MUs use the same transmit power $P_k = P_{MU}$. Other simulation parameters are presented in Table I. In our simulation, all the Monte Carlo simulations are obtained by performing 10^6 channel realizations. In addition, we compare the performance of the proposed BF scheme with ZF BF scheme and non-robust BF scheme:

- In ZF BF scheme, the intended signals are strengthened while interference is eliminated.
- In non-robust BF scheme, we obtain the BF vectors without considering the channel errors.

Fig. 3 and Fig. 4 show the impact of different transmit power on OP of the considered system. The pointing error parameters are assumed as $(\omega_z/a, \mu_x/a, \mu_y/a, \sigma_x/a, \sigma_y/a) = (10, 1, 2, 1, 2)$, and AoA uncertainty $\Delta = \theta_{l,U} - \theta_{l,L}$ is set as 1°. It can be observed that the simulation results are perfectly coincide with analytical results, confirming the validity of our theoretical analysis. As expected, the outage performance improves as transmit power increases. In Fig.3, the behavior of OP appears to be different in two regions. When the transmit power P_{MU} is below 25 dBmW, OP decreases with the increase of P_R, while if $P_{MU} > 25$ dBmW, OP contributes to a floor due to the dominant effect of FSO link in this region. A similar phenomenon occurs in Fig.4. When P_{MU} is fixed, the OP decreases with increasing aerial platform transmit power P_R and then falls to a constant when P_R exceeds a certain level. Moreover, this constant decreases with the increase of user transmit power P_{MU}. This is because when P_R is large enough, the OP is mainly determined by the RF link.

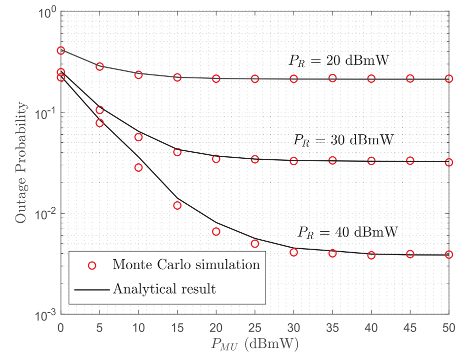

Fig. 3. OP versus user transmit power P_{MU} with different aerial platform transmit power P_R.

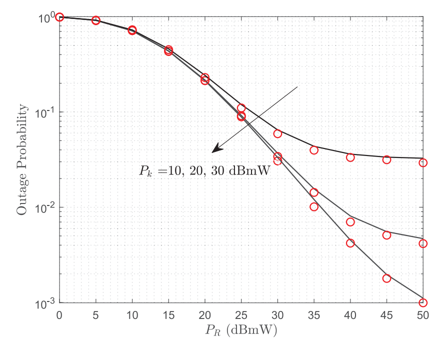

Fig. 4. OP versus aerial platform transmit power P_R with different user transmit power P_{MU}.

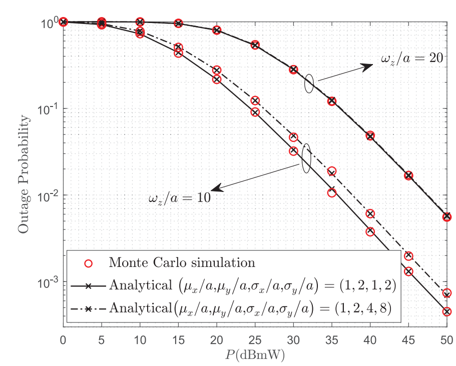

Fig. 5. OP versus transmit power P with different pointing errors.

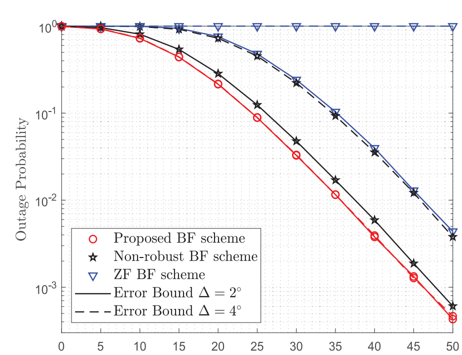

Fig. 6. OP versus transmit power P with different pointing errors.

Fig.5 presents the outage performance of the considered system under different pointing errors. We assume that the AoA uncertainty Δ is equal to 1°, and the aerial platform transmit power P_R is equal to user transmit power P_{MU} (i.e., $P_R = P_{MU} = P$). It can be observed that the outage performance degrades as a result of assuming much more severe pointing errors, such as normalized jitter values and normalized boresight errors. In addition, we also observe that the normalized beam width has an important impact on the outage performance.

Fig. 6 demonstrates the outage probability versus transmit power for different BF schemes. We take the ZF BF scheme and non-robust BF scheme as benchmarks. These BF schemes are based on the imperfect CSI. It can be found that the proposed BF scheme outperforms other two schemes, and its outage performance is not affected by the AoA angle uncertainty. This phenomenon indicates that our robust BF scheme can well handle the imperfect CSI in the RF link. Besides, when the AoA angle uncertainty is high, the performance of ZF and non-robust BF schemes is degraded, entailing that these two BF schemes are seriously deteriorated by channel uncertainties.

VI. Conclusion

In this paper, we have investigated the uplink transmission in a mixed RF-FSO satellite-aerial-terrestrial network. To ensure the quality of service for each user, we have designed a robust BF scheme to maximize the minimum average SINR of all the users. Then, by using the discretization method, H”older's inequality and Cauchy-Schwarz's inequality, we proposed an iterative algorithm to solve the BF optimization problem with the imperfect CSI in the RF links. Furthermore, we derived an analytical expression of OP based on the proposed BF algorithm. Finally, numerical results revealed that our proposed algorithm outperforms the existing works and can reduce the effect of the instability of aerial platform and the mobility of user in practice, thereby improving the system performance and robustness.

References

[1] E. Yaacoub and M. Alouini, “A key 6G challenge and opportunity-connecting the base of the pyramid: A survey on rural connectivity,” *Proc. IEEE*, vol. 108, no. 4, pp. 533–582, Apr. 2020.

[2] Q. Huang, M. Lin, W.-P. Zhu, J. Cheng, and M.-S. Alouini, “Uplink massive access in mixed RF/FSO satellite-aerial-terrestrial networks,” *IEEE Trans. Commun.*, vol. 69, no. 4, pp. 2413–2426, Apr. 2021.

[3] M. Horiuchi, H. Nishiyama, N. Kato, F. Ono, and R. Miura, “Throughput maximization for long-distance real-time data transmission over multiple UAVs,” in *Proc. IEEE Int. Conf. Commun.*, 2016, pp. 1–6.

[4] Z. Lin, M. Lin, T. de Cola, J.-B. Wang, W.-P. Zhu, and J. Cheng, “Supporting IoT with rate-splitting multiple access in satellite and aerial-integrated networks,” *IEEE Internet Things J.*, vol. 8, no. 14, pp. 11 123–11134, Jul. 2021.

[5] Y. Dong, M. Z. Hassan, J. Cheng, M. J. Hossain, and V. C. M. Leung, “An edge computing empowered radio access network with UAV-mounted FSO fronthaul and backhaul: Key challenges and approaches,” *IEEE Wireless Commun.*, vol. 25, no. 3, pp. 154–160, Jun. 2018.

[6] S. Chandrasekharan *et al.*, “Designing and implementing future aerial communication networks,” *IEEE Commun. Mag.*, vol. 54, no. 5, pp. 26–34, May 2016.

[7] K. Guo, M. Lin, B. Zhang, W. Zhu, J. Wang, and T. A. Tsiftsis, “On the performance of LMS communication with hardware impairments and interference,” *IEEE Trans. Commun.*, vol. 67, no. 2, pp. 1490–1505, Feb. 2019.

[8] K. Guo, K. An, F. Zhou, T. Tsiftsis, G. Zheng, and S. Chatzainotas, “On the secrecy performance of NOMA-based integrated satellite multiple-terrestrial relay networks with hardware impairments,” *IEEE Trans. Veh. Technol.*, vol. 70, no. 4, pp. 3661–3676, Apr. 2021.

[9] Q. Huang, M. Lin, W.-P. Zhu, S. Chatzinotas, and M.-S. Alouini, “Performance analysis of integrated satellite-terrestrial multiantenna relay networks with multiuser scheduling,” *IEEE Trans. Aerosp. Electron. Syst.*, vol. 56, no. 4, pp. 2718–2731, Aug. 2020.

[10] P. K. Sharma, D. Deepthi, and D. I. Kim, “Outage probability of 3-D mobile UAV relaying for hybrid satellite-terrestrial networks,” *IEEE Commun. Lett.*, vol. 24, no. 2, pp. 418–422, Feb. 2020.

[11] K. Gomez *et al.*, “Aerial base stations with opportunistic links for next generation emergency communications,” *IEEE Commun. Mag.*, vol. 54, no. 4, pp. 31–39, Apr. 2016.

[12] Q. Huang, M. Lin, J. Wang, T. A. Tsiftsis, and J. Wang, “Energy efficient beamforming schemes for satellite-aerial-terrestrial networks,” *IEEE Trans. Commun.*, vol. 68, no. 6, pp. 3863–3875, Jun. 2020.

[13] H. Kaushal and G. Kaddoum, “Optical communication in space: Challenges and mitigation techniques,” *IEEE Commun. Surv. Tut.*, vol. 19, no. 1, pp. 57–96, Jan.-Mar. 2017.

[14] V. Cazaubiel, G. Planche, V. Chorvalli, L. L. Hors, and E. Decourbey, “Lola: A 40000 km optical link between an aircraft and a geostationary satellite,” in *Proc. Int. Conf. Space Opt. Estec Noordwijk Netherlands*, 2006, pp. 1–6.

[15] M. Li, Y. Hong, C. Zeng, Y. Song, and X. Zhang, “Investigation on the UAV-to-satellite optical communication systems,” *IEEE J. Sel. Areas Commun.*, vol. 36, no. 9, pp. 2128–2138, Sep. 2018.

[16] E. Lee, J. Park, D. Han, and G. Yoon, “Performance analysis of the asymmetric dual-hop relay transmission with mixed RF/FSO links,” *IEEE Photon. Technol. Lett.*, vol. 23, no. 21, pp. 1642–1644, Nov. 2011.

[17] S. Anees and M. R. Bhatnagar, “Performance of an amplify-and-forward dual-hop asymmetric RF-FSO communication system,” *IEEE/OSA J. Opt. Commun. Netw.*, vol. 7, no. 2, pp. 124–135, Feb. 2015.

[18] H. Lei *et al.*, “On secure mixed RF-FSO systems with TAS and imperfect CSI,” *IEEE Trans. Commun.*, vol. 68, no. 7, pp. 4461–4475, Jul. 2020.

[19] Y. F. Al-Eryani, A. M. Salhab, S. A. Zummo, and M. Alouini, “Protocol design and performance analysis of multiuser mixed RF and hybrid FSO/RF relaying with buffers,” *IEEE/OSA J. Opt. Commun. Netw.*, vol. 10, no. 4, pp. 309–321, Apr. 2018.

[20] N. Varshney and P. Puri, “Performance analysis of decode-and-forward-based mixed MIMO-RF/FSO cooperative systems with source mobility and imperfect CSI,” *J. Lightw. Technol.*, vol. 35, no. 11, pp. 2070–2077, 2017.

[21] H. Kong, M. Lin, W. P. Zhu, H. Amindavar, and M. S. Alouini, “Multiuser scheduling for asymmetric FSO/RF links in satellite-UAV-terrestrial networks,” *IEEE Wireless Commun. Lett.*, vol. 9, no. 8, pp. 1235–1239, Aug. 2020.

[22] X. Liu, M. Lin, W. P. Zhu, J. Y. Wang, and P. K. Upadhyay, “Outage performance for mixed FSO-RF transmission in satellite-aerial- terrestrial networks,” *IEEE Photon. Technol. Lett.*, vol. 32, no. 21, pp. 1349–1352, Nov. 2020.

[23] A. Jurado-Navas, J. M. Garrido-Balsells, J. F. Paris, A. Puerta-Notario, and J. Awrejcewicz, “A unifying statistical model for atmospheric optical scintillation,” *Numer. Simulations Phys. Eng. Processes*, vol. 181, 2011.

[24] R. Boluda-Ruiz, A. García-Zambrana, C. Castillo-Vázquez, and B. Castillo-Vázquez, “Novel approximation of misalignment fading modeled by beckmann distribution on free-space optical links,” *Opt. Exp.*, vol. 24, no. 20, pp. 22635–22649, Oct. 2016.

[25] Z. Lin, M. Lin, J. Wang, Y. Huang, and W. Zhu, “Robust secure beamforming for 5 G cellular networks coexisting with satellite networks,” *IEEE J. Sel. Areas Commun.*, vol. 36, no. 4, pp. 932–945, Apr. 2018.

[26] I. S. Gradshteyn and I. M. Ryzhik, in *Table of Integrals, Series, and Products*, 8th ed. New York, NY, USA: Academic Press, 2014.

[27] A. P. Prudnikov, Y. A. Brychkov, and O. I. Marichev, *Integrals and Series*. New York, NY, USA: Gordon & Breach Science Publishers, 1990

[28] I. Wolfram, in *Research, Mathematica Edition: Version 8.0.* Champaign, IL, USA: Wolfram Research, 2010.